(Received 28 April 2025, Accepted 23 June 2025, Scheduled 5 July 2025)

A Microwave Imaging Solution to Inverse Scattering Problem using Distorted Born Iterative Method with Hybrid LSQR

Soumya Nharakkat*, Anjit T. Agamanandan, Anju Maria, and Mythili Palayyan

Division of Electronics engineering, School of Engineering, Cochin University of Science and Technology, Cochin 682022, India

ABSTRACT: Distorted Born Iterative Method (DBIM) is a deterministic iterative method which exhibits second-order convergence indicating that the reconstruction error decreases quadratically with successive iterations. Existing regularization techniques when being applied with DBIM often face challenges in determining the optimal regularization parameter (λ), leading to inconsistent convergence across various problems. To address this, a quantitative imaging algorithm is proposed in this paper by combining DBIM and Hybrid LSQR method for solving Inverse Scattering Problems (ISP). This enhances the accuracy of the reconstructed object profiles and optimizes the regularization level to prevent both under- and over-regularization. For a fair comparison with the results in the literature, simulation studies are conducted using a breast profile that has two tumor inclusions, each with a radius of 6 mm, and two fibro-glandular tissue inclusions, each with a radius of 10 mm. The proposed method achieves a Root Mean Square Error (RMSE) of 0.75, indicating a better level of accuracy. The experimental validation is performed using a phantom made of Delrin material. The Delrin phantom, with a diameter of 10 cm, contains three inclusions made of PVC material with diameters of 10 mm, 6 mm, and 3 mm. These inclusions have been successfully reconstructed with errors 0.085, 0.128, and 0.165, respectively. These results demonstrate the effectiveness of this algorithm in reconstructing both high and low-dielectric profiles, making it suitable for microwave imaging applications.

1. INTRODUCTION

In the modern era, Microwave Imaging (MWI) [1] plays a major role across various engineering and medical applications [2]. MWI utilizes electromagnetic waves in the microwave frequency range (300 MHz to 30 GHz) to solve Inverse Scattering Problems (ISPs). The goal of ISP is to determine the characteristics of the object under study by analyzing the dielectric variations based on the scattered electromagnetic waves. MWI has diverse applications in biomedicine, civil engineering [3, 4], Electro Magnetic Compatibility (EMC), geophysics, remote sensing, Non-Destructive Evaluation (NDE) [5], and structural health monitoring [6].

MWI methods are broadly classified into qualitative and quantitative approaches. Qualitative methods locate objects but do not provide precise measurements of material properties. Algorithms such as Synthetic Aperture Radar (SAR) [7], Delay-And-Sum (DAS) [8], and Multiple Signal Classification (MUSIC) [9] fall into this category. Meanwhile, quantitative methods reconstruct an object's shape, size, location, and dielectric values accurately. These methods are further divided into stochastic and deterministic approaches. Stochastic techniques [10–12] use probabilistic approaches. Deterministic methods [13–17] operate on fixed, predictable rules. Deterministic methods are preferred in well-defined scenarios with predictable uncertainties.

Among the deterministic methods, [18, 19] are limited to low dielectric contrasts. DBIM [16] offers a balance among computational efficiency, stability, and practical applicability, making it a preferred choice in MWI. DBIM provides stable convergence, is simpler to implement, and effectively reconstructs both low and high dielectric profiles. However, DBIM struggles with significant nonlinearity in ISP, leading to divergence in high-contrast scenarios. To address this, regularization techniques are essential to stabilizing solutions in large-scale and noisy imaging applications.

Regularization methods are categorized into variational and iterative approaches. Variational regularization solves an optimization problem with explicit regularization terms, integrating prior knowledge into the reconstruction process. Techniques explained in [20–23] fall into this category. These methods effectively stabilize the inverse problems but are computationally intensive and sensitive to noise. Selecting appropriate regularization parameters is crucial, as improper tuning can lead to over-smoothing (removal of essential details) or under-smoothing (retention of noise and artifacts).

On the other hand, Iterative regularization methods progressively update the solution and achieve stability through early stopping. These methods are computationally efficient per iteration but requires an appropriate selection of stopping criteria to avoid overfitting (noise amplification) or underfitting (insufficient reconstruction). Algorithms such as the Iterative Shrinkage-Thresholding Algorithm (ISTA) [24] and its variants, FISTA [25] and SpaRSA [26], Landweber Method [27], Conjugate Gradient Methods [28] and LSQR [29] fall into this category. Although these methods offer flexibility in handling nonlinearities and large-scale problems, their convergence rates are low. Further these methods are sensitive to initialization and converges to local minima. LSQR (Least Square QR) is a

* Corresponding author: Soumya Nharakkat (soumyajinu@cusat.ac.in).

widely used iterative solver for large-scale linear least squares problems where a matrix is decomposed into an orthogonal and an upper triangular matrix which suffer from semiconvergence [30]. To overcome this, Tikhonov regularization, a variational technique, is used to stabilize the solutions to ill-posed problems by incorporating a regularization term into the objective. This Hybrid LSQR [31] is an approach which is a combination of LSQR, an iterative regularization and Tikhonov, a variational regularization. Here, regularization is applied after projecting the problem into the Krylov subspace, effectively controlling noise within a reduced-dimension.

This paper proposes an integrated technique which combines DBIM with Hybrid LSQR to achieve optimized regularization level thereby ensuring improved reconstruction accuracy and stability for the reconstructed object profile.

The paper is structured as follows. Section 2 details the reconstruction algorithm used. Section 3 validates the reconstruction results using experimental data, assessing the accuracy and reliability of the proposed method. Finally, Section 4 concludes the paper.

2. PROBLEM STATEMENT

The object under study is illuminated using Transverse Magnetic (TM) waves, and these incident waves are scattered around in all directions due to the inhomogeneity introduced by the object. The objective is to reconstruct the object profile from the scattered data recorded by the antennas using the proposed imaging algorithm, which combines the Distorted Born Iterative Method (DBIM) with a hybrid LSQR approach. In this section, the process of data acquisition from the antennas in the presence of object under study is explained in detail. In Section 2.1, the tomographic imaging setup and the formulation of the Electric Field Integral Equation (EFIE) equations from Maxwell's equations for solving ISP is explained. Section 2.2 describes the reconstruction algorithm, which employs DBIM with the hybrid projection method.

2.1. Tomographic Imaging arrangement and EFIE formulation

As depicted in Fig. 1, the tomographic imaging setup consists of two distinct regions: image domain and measurement domain. Image domain V encompasses the object of interest, characterized by permittivity ϵ, and a homogeneous background medium with permittivity ϵ_b. This domain is discretized into a grid of N elements to model dielectric variations. The distance from the origin to any point in the image domain is denoted by r, while the distance from origin to any point in the measurement domain is represented by r'. The space surrounding the object is the measurement domain, where transmitting antennas emit microwaves that propagate through the medium and interact with the object, causing scattering in various directions. The receiver antennas capture the scattered signals, which encode information about the dielectric properties of the object, and this process is known as the forward problem. Conversely, retrieving the dielectric profile of the object from the measured scattered data is referred to as the inverse problem.

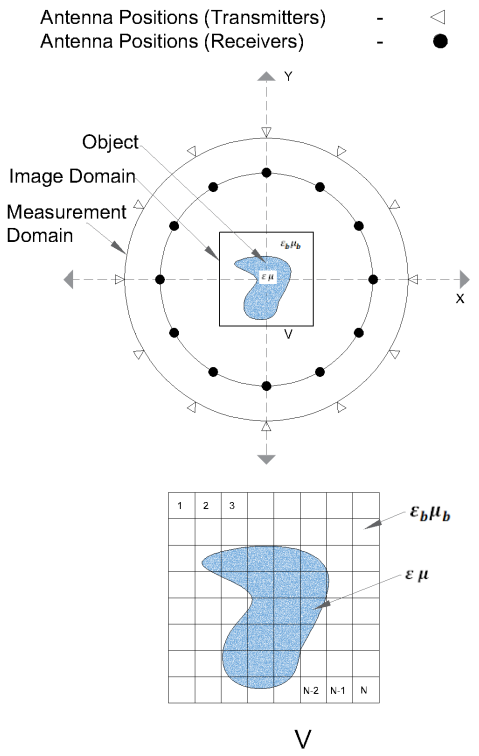

FIGURE 1. Tomographic imaging.

In any ISP, the dielectric characteristics of the object or scatterer are determined by solving the EFIE. However, the EFIE is nonlinear because the dielectric profile and the total electric field within the scatterer are simultaneously unknown. The total electric field at any given point on the scatterer is derived from Maxwell's wave equation and is expressed as [32]:

$$E^{\text{tot}}(r) = E^{\text{inc}}(r) + E^{\text{scat}}(r) \tag{1}$$

where $E^{\text{tot}}(r)$ is the total field in the medium with the presence of a scatterer, $E^{\text{inc}}(r)$ the incident field generated by the source at the background medium, and $E^{\text{scat}}(r)$ the scattered field due to scatterer-wave interaction.

$$E^{\text{tot}}(r) = E^{\text{inc}}(r) + j\omega\mu_b \int G(r, r') \cdot \tau(r') \cdot E^{\text{tot}}(r')\, dr' \tag{2}$$

From Equations (1) and (2), the scattered field is derived as [32]:

$$E^{\text{scat}}(r) = \omega^2\mu \int G(r, r').\tau(r').E^{\text{tot}}(r')\, dr' \tag{3}$$

where ω is the angular frequency, μ the scatterer permeability, μ_b the background permeability, G the Green's function, and τ the difference between the permittivity of the medium relative to the background.

$$\tau = \frac{\epsilon(r) - \epsilon_b(r)}{\epsilon_b(r)} \tag{4}$$

where τ is known as the contrast function. The Method of Moments (MoM) is used to discretize the EFIE. Equation (3) which

is the EFIE can be expressed in discrete form as [33]:

$$[E^{\text{scat}}] = [G][E^{\text{tot}}][\tau] \tag{5}$$

Equation (5) is solved to determine the dielectric profile of the object under investigation.

2.2. Proposed Reconstruction Technique

This paper employs a combination of DBIM with Hybrid LSQR which offers a better solution to the reconstruction problem.

The reconstruction steps involved in the DBIM-Hybrid LSQR method are:

1. Initialization of the dielectric values for the object profile.
2. The preliminary estimate of the object profile is determined using Born Approximation.
3. Iterations are carried out for solving EFIE.
   (a) In each iteration, the algorithm updates the dielectric profile and the total electric field.
   (b) Green's matrix is also updated based on the current estimate of the dielectric profile.
   (c) The optimal regularization parameter $\lambda_{k,\text{opt}}$ is determined for each iteration.
4. The algorithm iterates until the weighted Generalized Cross Validation [32] (GCV) stopping criteria is met.

This DBIM combined hybrid projection method offers an effective approach for solving ISP in microwave imaging. A key advantage of this method is that the search for an optimal regularization parameter is performed within the projected problem, which is of smaller dimension than the original large-scale problem. This reduction makes the computation significantly more efficient. In this approach, the regularization parameter is iteration-dependent, adapting dynamically as the Krylov subspace expands.

Hybrid LSQR method is incorporated from the IR tools package [31] in MATLAB R2024b which offers a variety of regularization methods that can provide optimal and stable solutions.

The hybrid nature of hybrid LSQR ensures robust and stable reconstructions, especially in cases where the inverse problem is ill-posed, or the data is noisy. By adjusting the regularization parameter and stopping criteria, hybrid LSQR offers a flexible framework for tackling a wide range of inverse problems.

The ISP explained in Equation (5) can be expressed in linear form as

$$Ax \approx b, \quad A \in \mathbb{R}^{M\times N}; \quad b \in \mathbb{R}^{M}, x \in \mathbb{R}^{N} \tag{6}$$

where A represents the measurement matrix which is $[G][E^{\text{tot}}]$; the product of Green's function and the total field, b, is the measured scattered data $[E^{\text{scat}}]$; x is the unknown contrast function; $\mathbb{R}^{M\times N}$ is the space of real-valued matrices with M rows and N columns; $\mathbb{R}^{M}$ is the space of real-valued vectors of length M; and $\mathbb{R}^{N}$ is the space of real-valued vectors of length N.

$$b = b^{\text{exact}} + e, \tag{7}$$

where b^{exact} denotes the noise-free data [34], and e is the noise. Inside the hybrid LSQR method, the Golub-Kahan bidiagonalization (GKB) process [34] is adopted. This process generates two sets of orthonormal vectors. These vectors span the Krylov subspaces $\mathcal{K}_k(A^\top A, A^\top b)$ and $\mathcal{K}_k(AA^\top, b)$. The initialization is done as follows:

$$u_1 = \frac{b}{\beta_1}, \quad v_1 = \frac{A^\top u_1}{\alpha_1}$$

where $\beta_1 = \|b\|$ with $\|\cdot\|$ being the standard Euclidean norm and

$$\alpha_1 = \|A^\top u_1\|.$$

At the kth iteration, the following recurrence relations hold:

$$AV_k = U_{k+1}B_k, \tag{8}$$

$$A^\top U_k = V_k B_k^\top + \alpha_{k+1} v_{k+1} e_k^\top, \tag{9}$$

where B_k is a lower bidiagonal matrix:

$$B_k = \begin{bmatrix} \alpha_1 & & & & \\ \beta_2 & \alpha_2 & & & \\ & \beta_3 & \alpha_3 & & \\ & & \ddots & \ddots & \\ & & & \beta_k & \alpha_k \\ & & & & \beta_{k+1} \end{bmatrix} \tag{10}$$

.

For $k \geq 1$, the new vectors and scalars u_{k+1} , v_{k+1} are computed as follows:

$$u_{k+1} = \frac{Av_k - \alpha_k u_k}{\beta_{k+1}}, \tag{11}$$

$$v_{k+1} = \frac{A^\top u_{k+1} - \beta_{k+1} v_k}{\alpha_{k+1}}, \tag{12}$$

where $\beta_{k+1} = \|Av_k - \alpha_k u_k\|$ and $\alpha_{k+1} = \|A^\top u_{k+1} - \beta_{k+1} v_k\|$.

These relations construct the bidiagonal matrix B_k, which forms the foundation for the iterative method. The kth iterate of the solution can be given as:

$$x_k(\lambda_k) = V_k(B_k^\top B_k + \lambda_k I_k)^{-1} B_k^\top U_{k+1}^\top b. \tag{13}$$

Note that $U_{k+1}^\top b = \|b\| e_1$. The regularization parameter λ_k is given as:

$$\lambda_k = \arg\min_{\lambda\in R_+} \|r(x(\lambda))\|^2 + 2\sigma^2 \text{ trace } \left(AA^\dagger_{\text{reg}}(\lambda)\right) - M\sigma^2, \tag{14}$$

where trace $\left(AA^\dagger_{\text{reg}}(\lambda_k)\right)$ is the trace of the influence matrix. It can be expressed as [34]:

$$AA^\dagger_{\text{reg}}(\lambda_k, k) = U_{k+1}B_k \left(B_k^\top B_k + \lambda_k I_k\right)^{-1} B_k^\top$$

Moreover, the norm of the residual is defined as:

$$r(x_k(\lambda_k)) = b - Ax_k(\lambda_k) = \left(I_m - AA^\dagger_{\text{reg}}(\lambda_k, k)\right) b$$

, and σ is the standard deviation of the noise e.

Weighted Generalized Cross-Validation (WGCV) method is an adaptive approach used to address over-smoothing issues by introducing a weight factor w, where $0 < w \leq 1$ to adjust the behavior of the GCV criterion.

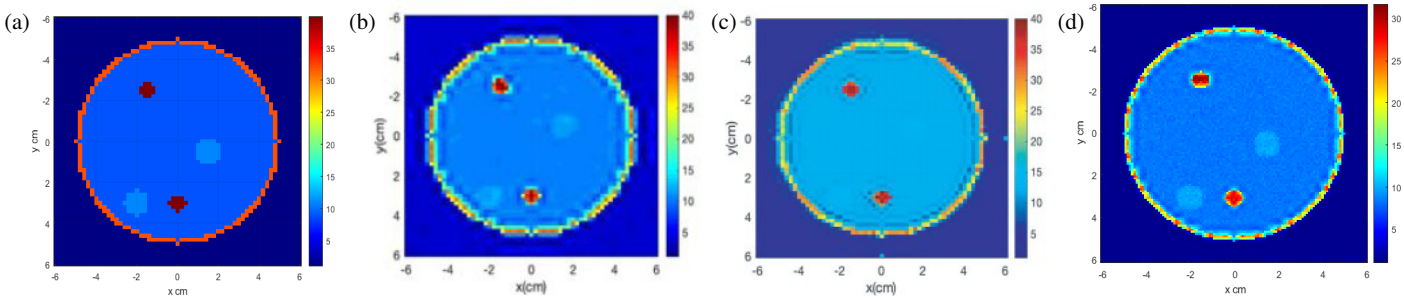

FIGURE 2. (a) Input Dielectric Profile : Profile-1, (b) Profile reconstructed by Weighted Basic Pursuit Algorithm (RwBP) at 3–4 GHz [35], (c) Profile reconstructed by SVBIM at 3–4 GHz [26], (d) Profile reconstructed by the Proposed method (DBIM with Hybrid LSQR) at 3–4 GHz.

At each iteration, weighted GCV [32] is given as:

$$G_w(\lambda_k, k) = \frac{n \left\| r(x_k(\lambda_k)) \right\|^2}{\left(\text{trace} \left(I_m - wAA^{\dagger}_{\text{reg}}(\lambda_k, k) \right) \right)^2}, \tag{15}$$

The optimal regularization parameter $\lambda_{k,\text{opt}}$ at the kth iteration is determined which satisfies the condition:

$$0 \leq \lambda_{k,\text{opt}} \leq \sigma_{\min}(B_k), \tag{16}$$

where $\sigma_{\min}$ denotes the smallest singular value of the matrix B_k. By minimizing the weighted GCV function with respect to w, the weight factor w can be determined.

$$\frac{\partial}{\partial w} \left(G_w(\lambda_k, k) \right) \Big|_{\lambda_k = \lambda_{k,\text{opt}}} = 0. \tag{17}$$

If $\sigma_{\min}(B_k)$ approaches zero in the later iterations due to ill-conditioning, the weight factor w can be approximated as the average of its previous values: $w_k = \text{mean}\{w_1, w_2, \ldots, w_k\}$.

At each iteration, the stopping criterion (17) is checked. When it is met, the solution $x_k(\lambda_k)$ can be calculated from the corresponding λ_k.

Simulation and experimental studies are conducted to assess the performance of the proposed method. The reconstruction results obtained from solving the ISP are presented in Section 3. The algorithm defined as Algorithm 1 is employed for the implementation of the proposed reconstruction method.

Algorithm 1 Proposed Reconstruction Algorithm

Require: Measured scattered data **b**, Measurement matrix A
1: Initialize dielectric profile $\mathbf{x}_0$, Iteration index, $k = 1$
2: **while** stopping criterion not satisfied **do**
3: Expand the projection subspace ran($\mathbf{V}_k$)
4: Compute $\mathbf{U}_{k+1}$ using β_{k+1}
5: Compute $\mathbf{V}_{k+1}$ using α_{k+1}
6: Compute regularization parameter λ_k
7: Evaluate the weighted GCV function
8: Update iteration index: $k \leftarrow k + 1$
9: **end while**
Ensure: **Approximate solution** $\mathbf{x}_k(\lambda_k)$

3. RESULTS AND DISCUSSION

Quantitative analysis is essential for assessing the effectiveness of the proposed method for solving the inverse scattering problem. In this context, the accuracy of reconstructed images is evaluated using Root Mean Square Error (RMSE). RMSE provides a measure of the average difference between the reconstructed image and the actual dielectric profile of the object under study and is expressed as [35]:

$$RMSE = \sqrt{\frac{1}{P} \sum_i \sum_j \left| \frac{\epsilon^r_{r_{i,j}} - \epsilon^t_{r_{i,j}}}{\epsilon^t_{r_{i,j}}} \right|^2} \tag{18}$$

where $\epsilon^r_{r_{i,j}}$ and $\epsilon^t_{r_{i,j}}$ denote the dielectric profiles reconstructed from the proposed method and the actual dielectric profile; $(i = 1, 2, \ldots, P_1;\ j = 1, 2, \ldots, P_2)$; and the total number of pixels $P = P_1 \times P_2$.

3.1. Simulation Results for the Proposed Technique

Two breast profiles, profile-1 and profile-2, with circular geometries consisting of a 5 mm thick outer skin layer and an inner fatty breast tissue layer with a 50 mm radius are considered for simulation studies. Two tumors, each measuring 6 mm in size, and two glandular inclusions, each 10 mm in size, are eccentrically embedded within the profiles, as illustrated in Fig. 2(a) and Fig. 3(a). Though the imaginary part has also been considered for the computations, only the real part of the dielectric profile is reported here, as it constitutes the primary quantity of interest for quantitative comparison and evaluation. The dielectric values of different tissues of breast profiles are given in Table 1. These values are taken as input to the proposed method for reconstructing the dielectric profile. These profiles are used in medical imaging research to mimic the properties of real breast tissue.

TABLE 1. Dielectric constants ε_r of tissues in breast profiles: Profile-1 and Profile-2.

Tissue Type [36, 37]	Profile-1 ε_r	Profile-2 ε_r
Skin	32	32
Fatty breast tissue	9	9
Fibrous tissue	11	11
Tumors	40	60

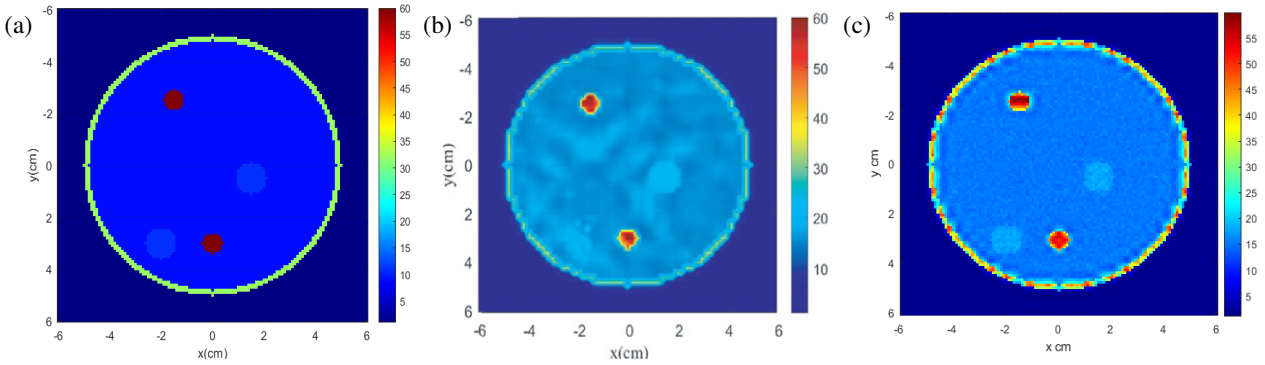

FIGURE 3. (a) Input Dielectric Profile : Profile-2, (b) Profile reconstructed by SVBIM at 3–4 GHz [26], (c) Profile reconstructed by the Proposed method (DBIM with Hybrid LSQR) at 3–4 GHz.

The number of transmitter and receiver antennas employed are 32. The frequency of operation is chosen as 3–4 GHz. The scattered data generated with the forward problem at 20 different frequencies have a size of $20 \times 32 \times 32$. An additive Gaussian noise of 30 dB signal-to-noise ratio (SNR) is incorporated here to account for typical noise intrusions present.

The algorithm processes the scattered data and generates the reconstructed images. To ensure a fair comparison, the results obtained using the proposed technique are quantitatively evaluated against existing studies in the literature. To assess the performance, RMSE is selected as the quantitative comparison metric. The reconstructed images are shown in Figs. 2(b)–2(d) and 3(b)–3(c). The comparison of the results of the proposed method with [26] and [35] for profile-1 are shown in Table 2 and with [26] for profile-2 in Table 3. The proposed method demonstrates improved accuracy in reconstructing the permittivity values of various breast tissues such as fatty adipose tissue, fibroglandular tissue, and tumor regions compared to both [26] and [35], resulting in reduced reconstruction error.

These findings indicate that the proposed method effectively reconstructs both high- and low-contrast scenarios. Consequently, the next step is to experimentally validate these numerical results. Details of the microwave imaging experiment and its corresponding results are discussed in Section 3.2.

The impact of noise on the reconstruction performance is evaluated by comparing the proposed method with RwBP and Total Variation (TV) Regularization [38] regularization techniques. The results shown in Fig. 4 demonstrate that the proposed method consistently outperforms both RwBP and TV regularization across all noise levels.

TABLE 2. Comparison of different methods for Profile-1.

Breast Model	Method	Permittivity, ε_r	RMSE
Tumor $\varepsilon_r = 40$	RwBP [35]	39.29	0.710
	SVBIM [26]	39.53	0.470
	Proposed method	**39.657**	**0.343**
Breast tissue $\varepsilon_r = 9$	RwBP [35]	8.35	0.650
	SVBIM [26]	8.59	0.410
	Proposed method	**8.66**	**0.340**
Glandular tissue $\varepsilon_r = 11$	RwBP [35]	10.31	0.690
	SVBIM [26]	10.54	0.460
	Proposed method	**10.655**	**0.345**

TABLE 3. Comparison of different methods for Profile-2.

Breast Tissue	Method	Permittivity, ε_r	RMSE
Tumor $\varepsilon_r = 60$	SVBIM [26]	59.13	0.872
	Proposed method	**59.25**	**0.750**
Breast tissue $\varepsilon_r = 9$	SVBIM [26]	8.46	0.540
	Proposed method	**8.54**	**0.460**
Glandular tissue $\varepsilon_r = 11$	SVBIM [26]	10.21	0.790
	Proposed method	**10.46**	**0.540**

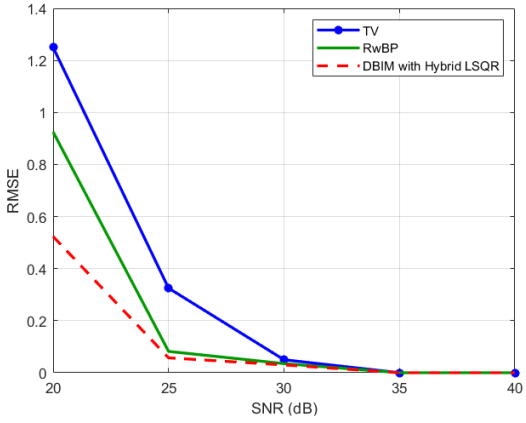

FIGURE 4. RMSE of reconstructed profile for different noise levels.

3.2. Validation with Experimental Results

For a fair comparison, the validation of the proposed reconstruction algorithm is done with a Delrin phantom. The Delrin phantom [39] used in the experiment is depicted in Fig. 5. The phantom has a cylindrical shape with a diameter of 10 cm and a height of 15 cm. The material chosen for this phantom is Delrin with a relative permittivity ($\varepsilon_r = 3.7$). The outer region of the phantom represents fatty breast tissues. The phantom contains three inclusions made of polyvinyl chloride (PVC) material, each with a higher permittivity ($\varepsilon_r = 4.8$). The inclusions mimic tumors and have varying sizes: 10 mm, 6 mm, and 3 mm.

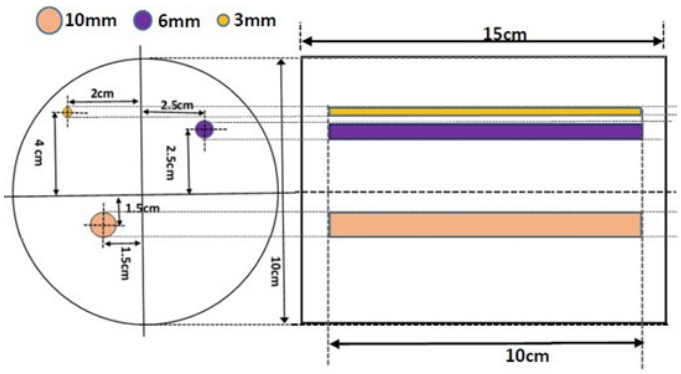

FIGURE 5. Inclusion details of Delrin Phantom.

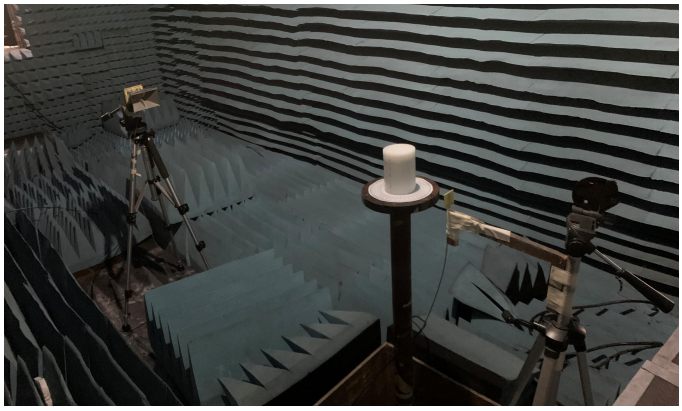

FIGURE 6. Experiment setup.

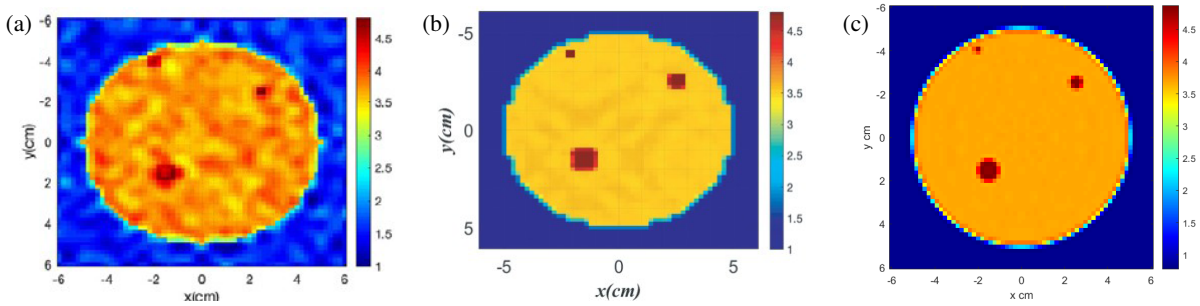

FIGURE 7. Reconstructed profiles of Delrin Phantom (a) by RwBP [35], (b) by SVBIM [26], (c) by the proposed method (DBIM with Hybrid LSQR).

TABLE 4. Comparison of inclusion localization and size estimation using the proposed method versus [26] and [35] for Delrin Phantom.

Inclusion 1 (Diameter = 10 mm, True Location = (1.5, 1.5))			
Method	**Location**	**Estimated Diameter (mm)**	**Error**
Proposed	**(1.503, 1.504)**	**9.15**	**0.085**
Ref. [26]	(1.505, 1.505)	9.11	0.089
Ref. [35]	(1.505, 1.515)	8.32	0.166
Inclusion 2 (Diameter = 6 mm, True Location = (2.5, 2.5))			
Method	**Location**	**Estimated Diameter (mm)**	**Error**
Proposed	**(2.51, 2.50)**	**5.24**	**0.128**
Ref. [26]	(2.51, 2.50)	5.2	0.133
Ref. [35]	(2.48, 2.50)	3.8	0.58
Inclusion 3 (Diameter = 3 mm, True Location = (2, 4))			
Method	**Location**	**Estimated Diameter (mm)**	**Error**
Proposed	**(2, 4)**	**2.34**	**0.165**
Ref. [26]	(2, 4)	2.2	0.21
Ref. [35]	(1.97, 4.012)	1.9	0.36

The experimental arrangement is given in Fig. 6. A standard horn antenna operating in the 2–18 GHz range is used as the transmitter antenna. The receiver antenna used is a microstrip UWB antenna of egg-shaped geometry [39]. Imaging is carried out by placing the receiver antenna at an angular spacing of 10 degrees, that is, at 36 locations around the phantom. PNAE 8362B vector network analyzer (Agilent Technologies, USA) was utilized for exciting the transmitter antenna between 3 and 10 GHz in the UWB frequency range at 201 discrete frequencies. The microwave signals are scattered by the phantom because of the inhomogeneity created by the inclusions with a dielectric constant different from that of the outer layer. The scattered signals are received by the receiver antenna. The above experiment is carried out inside an anechoic chamber. The proposed method is applied to the scattered data for the reconstruction of the scattered profile.

The reconstructed profiles for various methods are shown in the Figs. 7(a)–7(c).

The proposed method provides a more accurate estimate of the diameter of inclusion, resulting in smaller error values (Table 4). The improved dielectric value localization and size estimation, in comparison to [26] and [35], demonstrate the effectiveness of the proposed method.

4. CONCLUSION

An integrated quantitative reconstruction method combining the Distorted Born Iterative Method (DBIM) with Hybrid LSQR for solving Inverse Scattering Problems (ISP) is proposed in this paper. The proposed method is capable of reconstructing materials with both low and high dielectric contrasts, achieving values up to ε_r as high as 60. This imaging technique produces a significantly reduced permittivity error

value of 0.343 in the reconstruction of tumor inclusions even in the presence of 30 dB noise against 0.47 of Subspace-based Virtual Born Iteration Method (SVBIM) with SpARSA technique. Experimental validation is carried out using a Delrin phantom containing three inclusions measuring 10 mm, 6 mm, and 3 mm. The inclusions are successfully localized with errors of 0.085, 0.128, and 0.165, respectively.

This experimental validation demonstrates that the proposed method can detect inclusions of various sizes with minimal error, highlighting its potential for medical and industrial imaging applications. Although this study is limited to 2D imaging with Transverse Magnetic (TM) polarization, future work will focus on extending the approach to 3D imaging using Transverse Electric (TE) or full-vectorial illumination. This advancement will require modeling complex 3D field interactions, constructing appropriate 3D Green's matrices, and solving large-scale inverse problems to reconstruct the complete volumetric dielectric profile.

REFERENCES

[1] Dey, S. and A. O. Asok, "A review on microwave imaging for breast cancer detection," in *2024 IEEE Wireless Antenna and Microwave Symposium (WAMS)*, 1–5, Visakhapatnam, India, 2024.

[2] Khalid, N., M. Zubair, M. Q. Mehmood, and Y. Massoud, "Emerging paradigms in microwave imaging technology for biomedical applications: Unleashing the power of artificial intelligence," *Npj Imaging*, Vol. 2, No. 1, 13, 2024.

[3] Mikhnev, V. and P. Vainikainen, "Microwave imaging of layered structures in civil engineering," in *2002 32nd European Microwave Conference*, 1–4, Milan, Italy, 2002.

[4] Feng, M. Q., F. D. Flaviis, and Y. J. Kim, "Use of microwaves for damage detection of fiber reinforced polymer-wrapped concrete structures," *Journal of Engineering Mechanics*, Vol. 128, No. 2, 172–183, 2002.

[5] Lockwood, S. J. and H. Lee, "Pulse-echo microwave imaging for NDE of civil structures: Image reconstruction, enhancement, and object recognition," *International Journal of Imaging Systems and Technology*, Vol. 8, No. 4, 407–412, 1997.

[6] Li, Z., C. Soutis, A. Haigh, R. Sloan, A. Gibson, and N. Karimian, "Microwave imaging for delamination detection in T-joints of wind turbine composite blades," in *2016 46th European Microwave Conference (EuMC)*, 1235–1238, London, UK, 2016.

[7] Liao, Y., Z. Zhou, and F. Tian, "Microwave imaging system based on synthetic aperture radar algorithm," in *2023 IEEE 6th Information Technology,Networking,Electronic and Automation Control Conference (ITNEC)*, Vol. 6, 281–284, Chongqing, China, 2023.

[8] Yashaswini, P., U. Singh, and J. Mukherjee, "Enhancing early-stage breast cancer detection: Antenna design, realistic phantom modeling, and multi-static imaging with DAS algorithm," in *2024 11th International Conference on Signal Processing and Integrated Networks (SPIN)*, 409–414, Noida, India, 2024.

[9] Park, W.-K., "Application of MUSIC algorithm in real-world microwave imaging of unknown anomalies from scattering matrix," *Mechanical Systems and Signal Processing*, Vol. 153, 107501, 2021.

[10] Etminan, A. and M. Moghaddam, "Microwave imaging of dielectric objects using a combination of simulated annealing and multi-directional search," in *2017 IEEE International Symposium on Antennas and Propagation & USNC/URSI National Radio Science Meeting*, 2371–2372, San Diego, CA, USA, 2017.

[11] Mhamdi, B., K. Grayaa, and T. Aguili, "Microwave imaging of dielectric cylinders from experimental scattering data based on the genetic algorithms, neural networks and a hybrid micro genetic algorithm with conjugate gradient," *AEU — International Journal of Electronics and Communications*, Vol. 65, No. 2, 140–147, 2011.

[12] Randazzo, A., "Swarm optimization methods in microwave imaging," *International Journal of Microwave Science and Technology*, Vol. 2012, No. 1, 491713, 2012.

[13] Bilgin, E., S. Doğu, S. Coşğun, and M. Çayören, "A modified newton method formulation for microwave imaging," in *2020 IEEE Asia-Pacific Microwave Conference (APMC)*, 1057–1059, Hong Kong, 2020.

[14] Nordebo, S. and M. Gustafsson, "A priori modeling for gradient based inverse scattering algorithms," *Progress In Electromagnetics Research B*, Vol. 16, 407–432, 2009.

[15] Tajik, D., A. D. Pitcher, and N. K. Nikolova, "Comparative study of the rytov and born approximations in quantitative microwave holography," *Progress In Electromagnetics Research B*, Vol. 79, 1–19, 2017.

[16] Amin, B., A. Shahzad, M. O'halloran, B. Mcdermott, and A. Elahi, "Experimental validation of microwave imaging prototype and dbim-imatcs algorithm for bone health monitoring," *IEEE Access*, Vol. 10, 42 589–42 600, 2022.

[17] Diao, H., H. Liu, Q. Meng, and L. Wang, "Effective medium theory for embedded obstacles in electromagnetic scattering with applications," *Journal of Differential Equations*, Vol. 437, 113283, 2025.

[18] Vargas, J. O. and R. Adriano, "Subspace-based conjugate-gradient method for solving inverse scattering problems," *IEEE Transactions on Antennas and Propagation*, Vol. 70, No. 12, 12 139–12 146, 2022.

[19] Ireland, D., K. Bialkowski, and A. Abbosh, "Microwave imaging for brain stroke detection using born iterative method," *IET Microwaves, Antennas & Propagation*, Vol. 7, No. 11, 909–915, 2013.

[20] Mousavi, S. S. S. and M. S. Majedi, "A quantitative microwave imaging approach for brain stroke classification based on the generalized tikhonov regularization," *IEEE Access*, Vol. 11, 73 370–73 376, 2023.

[21] Yaswanth, K. and U. K. Khankhoje, "Two-dimensional nonlinear microwave imaging with total variation regularization," in *2017 Progress in Electromagnetics Research Symposium — Fall (PIERS — FALL)*, 1509–1513, Singapore, 2017.

[22] Khajehnejad, M. A., W. Xu, A. S. Avestimehr, and B. Hassibi, "Weighted ℓ 1 minimization for sparse recovery with prior information," in *2009 IEEE International Symposium on Information Theory*, 483–487, Seoul, Korea (South), 2009.

[23] Shah, P., U. K. Khankhoje, and M. Moghaddam, "Inverse scattering using a joint $L1$–$L2$ norm-based regularization," *IEEE Transactions on Antennas and Propagation*, Vol. 64, No. 4, 1373–1384, 2016.

[24] Bayram, □., "On the convergence of the iterative shrinkage/thresholding algorithm with a weakly convex penalty," *IEEE Transactions on Signal Processing*, Vol. 64, No. 6, 1597–1608, 2016.

[25] Beck, A. and M. Teboulle, "A fast iterative shrinkage-thresholding algorithm for linear inverse problems," *SIAM Journal on Imaging Sciences*, Vol. 2, No. 1, 183–202, 2009.

[26] Benny, R., T. A. Anjit, P. Cherian, and P. Mythili, "A combinatorial approach to quantitative microwave imaging for breast tumour profiling using SVBIM and SpaRSA," *Progress In Elec-*

tromagnetics Research C, Vol. 139, 45–57, 2024.

[27] Al-Mahdawi, H. K. I., H. Alkattan, M. Abotaleb, A. Kadi, and E.-S. M. El-kenawy, "Updating the landweber iteration method for solving inverse problems," *Mathematics*, Vol. 10, No. 15, 2798, 2022.

[28] Cui, T. J., W. C. Chew, A. A. Aydiner, and S. Chen, "Inverse scattering of two-dimensional dielectric objects buried in a lossy earth using the distorted born iterative method," *IEEE Transactions on Geoscience and Remote Sensing*, Vol. 39, No. 2, 339–346, 2001.

[29] Huang, Y. and Z. Jia, "Some results on the regularization of LSQR for large-scale discrete ill-posed problems," *Science China Mathematics*, Vol. 60, 701–718, 2017.

[30] Gazzola, S. and P. Novati, "Automatic parameter setting for Arnoldi-Tikhonov methods," *Journal of Computational and Applied Mathematics*, Vol. 256, 180–195, 2014.

[31] Gazzola, S., P. C. Hansen, and J. G. Nagy, "IR Tools: A MATLAB package of iterative regularization methods and large-scale test problems," *Numerical Algorithms*, Vol. 81, No. 3, 773–811, 2019.

[32] Chung, J., J. G. Nagy, D. P. O'leary, *et al.*, "A weighted GCV method for Lanczos hybrid regularization," *Electronic Transactions on Numerical Analysis*, Vol. 28, No. 149-167, 2008, 2008.

[33] Yaswanth, K., S. Bhattacharya, and U. K. Khankhoje, "Algebraic reconstruction techniques for inverse imaging," in *2016 International Conference on Electromagnetics in Advanced Applications (ICEAA)*, 756–759, Cairns, QLD, Australia, 2016.

[34] Havelková, E. and I. Hnětynková, "Residual norm behavior for Hybrid LSQR regularization," *Programs and Algorithms of Numerical Mathematics, Proceedings of Seminar*, 65–74, Institute of Mathematics CAS, Prague, Czech Republic, 2023.

[35] Anjit, T., R. Benny, P. Cherian, and M. Palayyan, "Microwave imaging solutions for medical imaging using re-weighted basic pursuit algorithm," *Progress In Electromagnetics Research M*, Vol. 97, 13–24, 2020.

[36] Tavassolian, N., H. Kanj, and M. Popovic, "Assessment of Dark eyes antenna radiation in the vicinity of the realistic breast model," in *12th International Symposium on Antenna Technology and Applied Electromagnetics (ANTEM)*, 2006.

[37] Fear, E. C. and M. Okoniewski, "Confocal microwave imaging for breast tumor detection: Application to a hemispherical breast model," in *2002 IEEE MTT-S International Microwave Symposium Digest (Cat. No.02CH37278)*, Vol. 3, 1759–1762, Seattle, WA, USA, 2002.

[38] Jamali, N. H., K. A. H. Ping, S. Sahrani, and T. Takenaka, "Image reconstruction based on combination of inverse scattering technique and total variation regularization method," *Indonesian Journal of Electrical Engineering and Computer Science*, Vol. 5, No. 3, 569–576, 2017.

[39] Cherian, P., T. A. Anjit, and P. Mythili, "A compact egg-shaped UWB antenna for breast dielectric profile imaging," *International Journal of Scientific & Technology Research*, Vol. 9, No. 03, 4672–4681, 2020.